Evidence for a magnetic-field-induced Wigner glass in the two-dimensional electron system in Si inversion layers

B. A. Wilson, S. J. Allen, Jr., and D. C. Tsui

Bell Laboratories, Murray Hill, New Jersey 07974

(Received 6 March 1981)

Cyclotron resonance experiments on the two-dimensional electron system in Si inversion layers are described that probe the dynamical response in the extreme quantum limit. A remarkable narrowing and shifting of the absorption line is observed as the electron density n_s is reduced to the point that only the lowest spin-valley-Landau level is occupied. This anomalous behavior has been studied as a function of magnetic field ($B \leq 7.5$ T), electron density ($n_s \geq 10^{10}/cm^2$), temperature (1.2−30 K), and substrate bias (surface electric field). The spectroscopy is performed with a Michelson interferometer which determines conductivity $\sigma(\omega)$ from 5 to 60 cm^{-1} with all the external parameters of the system, in particular the magnetic field, held fixed. The results are compared with a variety of models including single-electron trapping, electron-phonon coupling, and a pinned charge-density wave (CDW). Although all suffer some shortcomings, the most satisfactory account of the experimental results is obtained by assuming that the electrons form some sort of short-range-ordered structure at low temperatures in the extreme quantum limit. A quantitative comparison is made with the pinned-CDW model of Fukuyama and Lee. Fitting this model to the experimental data results in a pinning parameter that depends inversely on wave-function thickness normal to the interface. The modulation depth of the CDW and the correlation length of the short-range order are also extracted. The picture that emerges in the extreme quantum limit is that of a highly disordered Wigner glass.

I. INTRODUCTION

At low densities and low temperatures the behavior of an electron gas is dominated by electron-electron correlations, leading to crystallization into a Wigner lattice.[1,2] Current speculation is that strong magnetic fields enhance the formation of such a correlated ground state.[3−13] In the extreme quantum limit, where only the ground Landau level is occupied, the kinetic energy associated with the electron degeneracy is quenched and the electron-electron interactions must overcome only the thermal kinetic energy to produce a crystallized ground state. As a result, in the extreme quantum limit, electrons are expected to behave as classical particles, crystallizing at sufficiently low temperature. The ability to vary the electron density at will in the two-dimensional (2D) electron gas found in Si inversion layers makes it an attractive system in which to explore this possibility.

There have been a number of dc transport measurements in Si metal-oxide−semiconductor field-effect transistors (MOSFET's) that suggest singular behavior in the lowest Landau level. Kawaji

et al.[14,15] have observed two activation energies in the dc conductivity, and suggest that this behavior is caused by a pinned Wigner solid. Tsui[16] has also reported anomalies in the magnetotransport that are sensitive to the measuring electric field. The cyclotron resonance data of Kennedy et al.[17−19] previewed the behavior described below; they observed line narrowing and shifting in the quantum limit.

The theoretical developments which have guided our thinking are best described with reference to Fig. 1. Here we show theoretical phase diagrams for the 2D electron gas in a 7.5 T magnetic field. The lines indicate various predictions of the phase boundary in the temperature filling factor plane between regions of electron solid and fluid. The filling factor v is the fractional occupancy of the lowest spin-valley-Landau level and is given by $v = n_s h/eB$ or $v = n_s 2\pi l^2$ where l is the cyclotron radius and n_s is the electron density.

In arbitrarily large fields we expect the classical result to hold and this is shown by the low-lying parabolic curve in Fig. 1. The recent experiments of Grimes and Adams[2] which demonstrated
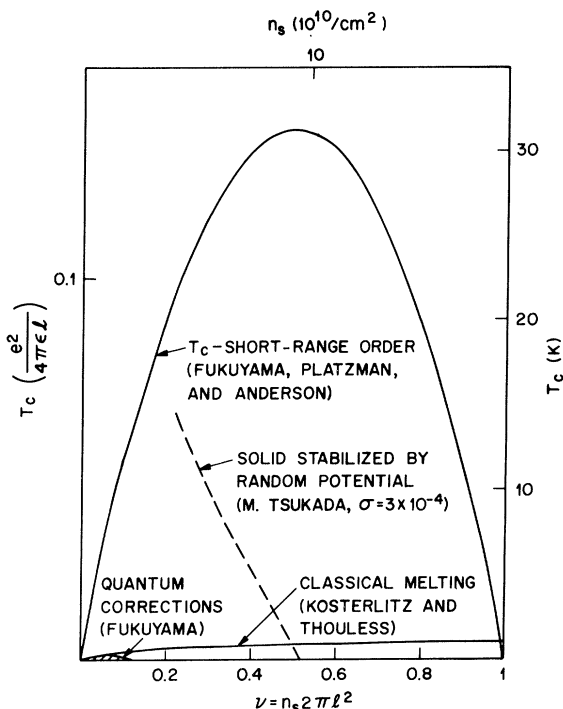
n_s $(10^{10}/cm^2)$

FIG. 1. Theoretical predictions of the phase diagram of the 2D electron gas in the extreme quantum limit.

Wigner crystallization of the 2D electron gas on liquid helium, fix this curve at temperatures well below the temperatures achieved in these experiments. These temperatures have been shown to be consistent with the Kosterlitz-Thouless[20−24] mechanism of 2D melting due to spontaneous formation of defects, especially after suitable corrections are included that predict a softening of the lattice at elevated temperatures.[25]

In a finite magnetic field Fukuyama[13] has shown that quantum fluctuations further suppress the ordering temperature, which for Si inversion layers restricts the allowed region of the v, T plane to the hatched region indicated in Fig. 1. The phase boundary approaches the classical curve for $v \ll 1$ but probably precludes a transition for $v \gtrsim 0.1$.

A more optimistic statement is made by Fukuyama, Platzman, and Anderson[12], who argue that at higher temperatures one might observe substantial short-range order provided that the temperature and density of the system lie within the bell-shaped curve shown in Fig. 1. The range of temperature and density encompassed by this short-range-ordered phase is more than an order of magnitude larger than that allowed by the classical

theory with quantum corrections.[13]

Also of interest is the theory of Tsukada[6,7] who has modeled the effect of a random disordering potential on the phase diagram. The presence of pinning potentials stiffens the lattice and increases the transition temperature to a solid state. Although his theory, based on a self-consistent calculation of the transverse sound velocity, does not agree with the dislocation theory of melting, it does draw our attention to the importance of random pinning potentials and the fact that they may help stabilize the electron solid. Although restricted to $T = 0$ K, computer simulations by Aoki[10] have demonstrated the Wigner crystallization in a magnetic field and the influence of disorder upon it. We anticipate our conclusions and point out that in this system the magnitude of the disordering potential is not small compared with the Coulomb interaction energy between electrons, and must be considered in any quantitative modeling of the ground state.

All of the above theories assume that the cyclotron energy is much larger than the Coulomb interaction which in turn must be much larger than the disordering potential. In the following it will prove to be the case that this condition is only weakly satisfied as the energies are of comparable magnitude. In the last analysis this mitigates any rigorous confrontation between experiment and theory.

The probe that we have used to examine the 2D electron gas in the extreme quantum limit is cyclotron resonance (CR), which has been the subject of a number of investigations in Si MOSFET's.[17−19,26−34] In principle CR should give unambiguous measure of the electron mass and scattering rate. Historically, however, for (100) surfaces the resonance is seldom consistent with the bulk mass of 0.1905 or related simply to the zero magnetic field scattering rate determined from the dc conductivity.

In earlier publications[35,36] we briefly reported the results of CR experiments in the two-dimensional electron gas in Si inversion layers produced in a Si MOSFET in the quantum limit. The width and position of CR were shown to exhibit a remarkable quantum effect that strongly suggests a condensation of the electron gas into a highly correlated ground state, if not a lattice, when the first Landau level is only paritally occupied. In the following we discuss in some detail the experimental results as well as a number of models that we have examined in search of a coherent explanation of our observations.

TABLE I. Characteristics of samples.

Sample	Orientation	Peak mobility at 4.2 K (cm²/Vs) [at n_s (cm⁻²)]	Gate conductance (mho/□)	Oxide thickness (Å)	Electron density/volt (cm⁻² V⁻¹)	Flatband voltage (V)	Substrate doping (cm⁻³)	Fixed oxide charge (cm⁻²)	Gate oxidation
GKB9-8	100	12 000 [9.3×10^{11}]	0.0014	3680	5.75×10^{10}	-0.76	p:1.23×10^{15}	$\sim4\times10^{10}$	Wet
GKB9-9	100	16 000 [2.4×10^{11}]	0.00075	5230	4.04×10^{10}	-1.21	p:1.3×10^{15}	$\sim4\times10^{10}$	Wet
GK10/17/77	1° tilt from (100) in [110] direction	18 800 [$\sim8\times10^{11}$]	0.00725	11 200	1.88×10^{10}	-1.99	p:$\sim1\times10^{15}$	$\sim4\times10^{10}$	Dry
GK3/23/79	100	8 500 [8.8×10^{11}]	0.00535	920	2.3×10^{11}	-0.25	p:1.0×10^{15}	$\sim4\times10^{10}$	Dry

II. EXPERIMENTAL

A. Samples and apparatus

The experiments we report here were performed on the n-inversion layer of (100) oriented Si MOSFET's. The samples were of large area, 2.5×2.5 mm², and thin gate metallization, ~50 Å of Ti, to optimize IR transmission. Two terminal dc transport measurements were performed. The resulting characteristics of the samples are summarized in Table I.

The far-infrared conductivity was determined by measuring the fractional change in transmission through the device when the inversion layer electrons are introduced. The frequency dependence of the transmission was obtained with a standard Michelson Fourier transform spectrometer. Sample temperatures from 1.2 K to room temperature and magnetic fields up to 8.0 T were obtained by inserting the samples in a variable-temperature Dewar equipped with a superconducting magnet. Other details of the experimental setup have been described elsewhere[37] and will not be repeated here. Two points are, however, worth emphasizing. The experiment contains no unknown scaling factors, and thus yields an *absolute* measure of the conductivity. Also, unlike previously reported cyclotron resonance experiments,[17−19,26−35] we fix B as well as other system parameters, and observe $\sigma(\omega)$ with the spectrometer. The latter point is crucial. It will become apparent that the CR line shape and position depend on B in such a way that fixed laser frequency, swept magnetic field experiments at the quantum limit should be difficult to interpret.

It was found that the high peak mobility samples suffered severe contact problems at low temperatures and at densities below 10^{12}/cm². This leads to apparent localization at anomalously high electron densities accompanied by extremely nonlinear current-voltage (I-V) relations for the inversion layer. Remarkably, negative substrate bias removed the contact resistance, depressing the critical electron density below which thermal activation appears, and removing the extreme nonlinearities in the I-V. Details concerning this contact effect and the bearing on the problem of anomalous localization will be published elsewhere. In Fig. 2 we show $\log_{10}\sigma$ versus $1/T$ for a typical sample with sufficient negative substrate bias that there is no serious problem with the contact.

B. Magnetotransport

Magnetoconductivity measurements were made on the samples, both as a background for the
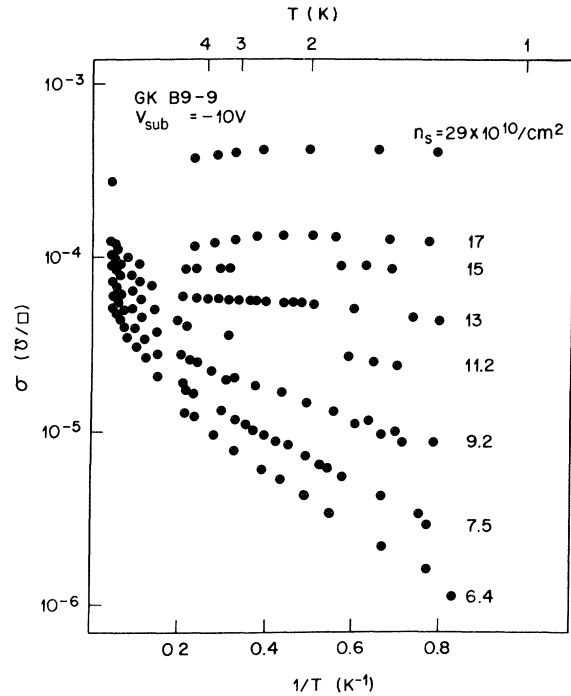
FIG. 2. Log σ vs $1/T$ for sample GKB9-9 with an *applied* substrate bias of -10 V. Contact effects are absent (mho/□ is 2D conductance per square).

FIG. 3. (a) Conductivity versus gate voltage V_g, with $B = 1.5 - 5$ T as a parameter. (b) Conductivity versus B with $n_s = 10^{12}$ cm^{-2}.

high-frequency CR studies and as a check of the charging threshold at low temperatures. The Shubnikov—de Haas (SdH) oscillations, which are small due to the square geometry of the devices, can be seen in either n_s or magnetic field scans. Typical examples are shown in Fig. 3. Swept magnetic field runs yield more consistent results for threshold since the size of the structure scales with field, allowing any part of the feature to be used as a reference point. Although the oscillations provide a clear measure of the density at large n_s, the validity of extrapolating these data into the localized regime in order to define a charging threshold, V_T, has often been questioned. For these samples, however, we find the extrapolated SdH values of V_T to be in good agreement with other measurement techniques, as discussed later.

C. Determination of threshold, electron density, and surface field

The most accurate determination of the charging threshold V_T, is obtained by measuring the broadband ir absorption due to the presence of the inversion layer electrons. This is accomplished by detecting the change in the total ir transmission when a voltage is applied to the gate, introducing electrons into the channel. As noted previously by
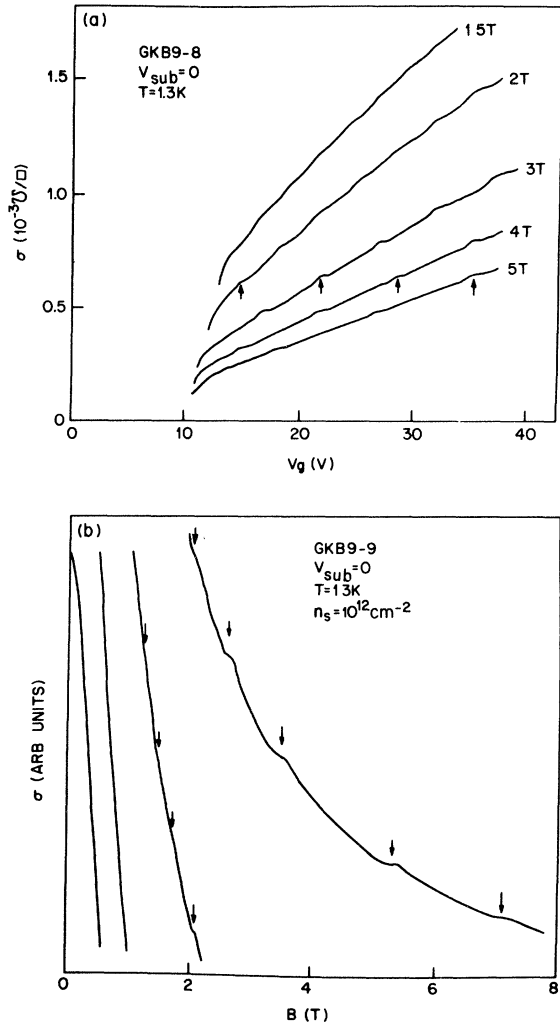
Wagner et al.,[18,19] this can be a very sensitive probe. We are able to see absorption by as few as 5×10^9 e/cm^2. Since we are not normalizing the signal by the frequency response of the system, the linearity of this technique depends on the absorption line shape and position remaining constant as n_s is increased. As we shall show later, the narrow invariant line shape of the CR in the extreme quantum limit satisfies this criterion, resulting in a simple linear growth of the ir absorption with the gate voltage V_G, and an accurate determination of V_T. Coupled with the known capacitance of the device, n_s is subsequently determined to an accuracy of approximately $\pm 10^{10}$/cm^2.

As with all measurements in this high-resistivity regime, one must be careful to allow the system

time to come to equilibrium. We have found that if the device is turned off hard by dropping V_G well below V_T so that the depletion layer as well as the inversion layer is discharged, equilibration of the inversion layer after reapplying a small positive gate voltage can be extremely slow—extending to hours in some cases. This can lead to apparent shifts of V_T with time, and to discrepancies between the values of V_T determined by ir absorption and extrapolation of SdH data taken in the "metallic" regime where the system response is fast. Such problems were apparently experienced by Wagner et al.[18,19] who observed a CR line shape and intensity that were not stable in time.

Fortunately this pitfall can be avoided, at least in some samples in which repopulation of the inversion layer is rapid, as long as the depletion layer is not disturbed. This is indicated by total agreement of ir threshold measurements on different time scales both with each other and with the extrapolated SdH data. By switching V_G only slightly below V_T for the background reference signal, we leave the depletion layer intact, reducing the depletion charge by $< 10^{10}/\text{cm}^2$, and the system equilibrates much faster than the 10 s gate-voltage switching time of our experiments.

From the observed threshold at zero substrate bias and the known substrate doping we can determine the flatband voltage, which is typically $\sim -1V$ in these samples. The threshold may be varied by the application of a substrate bias (V_{sub}), which provides a means of varying the electron density and surface field independently. At room temperature the threshold shift of our samples, ΔV_T, follows the expected relationship

$$\Delta V_T = \frac{[2\epsilon_s(N_A - N_D)/e]^{1/2}}{[(C/A)/e]}$$

$$\times [(V_S + V_{\text{sub}})^{1/2} - V_S^{1/2}], \qquad (1)$$

confirming the doping, $(N_A - N_D)$, of the substrate. In the numerator, ϵ_s is the Si dielectric permitivity and V_S the energy gap from the Fermi energy to the conduction band, adjusted for the ground-state energy of the lowest subband. The denominator is the capacitance per unit area of the device.

At low temperatures, 77 K and below, however, the observed threshold shift is noticeably smaller and deviates from this relationship, although it still responds rapidly to applied substrate bias. Other workers have reported long equilibration times when changing V_{sub} in the cold dark, but we see an abrupt change in the conductivity with no further changes on longer time scales, despite the fact that the depletion layer does not charge as completely as it does at 300 K. We also see no difference in V_T whether V_{sub} is applied at liquid N_2 and maintained during cooling, or applied abruptly at low temperature. The presence of room-temperature black-body radiation in our apparatus may aid the rapid charging of the sample. (Nevertheless, it is somewhat difficult to reconcile this rapid response to substrate bias with the slow recovery observed after the device has been turned off hard.) We conclude that the substrate-bias-induced threshold shift is less than obtained at 300 K, but stable. A possible explanation for the diminished substrate bias effect is a voltage drop between the substrate contact and the depletion layer due to the high resistivity of the substrate at low temperatures, resulting in an effective substrate bias that is only some fraction of that applied, empirically about 50%. This effect may be specific to the geometry of our devices in which the substrate contact is coplanar with the source and drain connections rather than on the back side of the substrate. At any rate, since the expected relation between V_T and the applied V_{sub} is not satisfied at low temperatures, we ignore it and simply use the empirically observed thresholds to determine the electron density and surface field.

The surface electric field is the sum of the inversion layer field at the interface and the depletion layer field which we calculate from the measured threshold shift and the known depletion layer doping. If the flatband voltage is V_{FB} then the depletion layer charge is

$$N_{\text{depl}} \cong (V_T - V_{\text{FB}})\frac{\epsilon_{\text{ox}}}{et_{\text{ox}}}, \qquad (2)$$

where ϵ_{ox} and t_{ox} are the dielectric constant and thickness of the oxide.

To estimate the wave-function thickness we use the variational wave function of Stern and Howard,[38]

$$\phi(z) = \left[\frac{b^3}{2}\right]^{1/2} z\, e^{-bz/2}, \qquad (3)$$

and minimize the ground-state energy of the following Hamiltonian:

$$\mathcal{H} = -\frac{\hbar^2}{2m}\frac{\partial^2}{\partial z^2} + (N_{\text{depl}} + \beta N_{\text{inv}})\frac{e^2 z}{\epsilon_s}$$

$$+ \frac{\epsilon_s - \epsilon_{\text{ox}}}{\epsilon_s + \epsilon_{\text{ox}}}\frac{e^2}{8\pi\epsilon_s z}. \qquad (4)$$

The last term is the image potential. β is a parameter that lies somewhere between 0 and 1. For our low-density data, $N_{depl} \gg N_{inv}$, and the exact value of β is not critical. In the following discussions we use $\beta = 1$ to determine b.

D. Zero magnetic field ir absorption

At large n_s in the "metallic" regime, the frequency-dependent conductivity measured by ir absorption exhibits a normal Drude behavior which agrees quantitatively with the dc transport data. At low densities, however, $\sigma(\omega)$ departs noticeably from Drude, peaking at a finite frequency, and in some cases falling somewhat too rapidly at higher frequencies. Applying a negative substrate bias pulls the peak to higher frequencies. A typical spectrum is shown in Fig. 4 for $V_{sub} = -30$ V. The dc value shown for comparison is a two-terminal measurement, but the negative substrate bias ameliorates any contact problems, giving ohmic behavior at all values of source drain electric fields below channel pinchoff, in agreement with four-terminal measurements. The small dc value of the conductivity is consistent with the turnover in $\sigma(\omega)$, but it is not possible to say definitively whether it correctly predicts the intercept of $\sigma(\omega)$ from the contactless ir measurements.

Although details of specific models for the absorption line shape will be discussed in a separate publication, it is important to realize that a departure from Drude implies a frequency-dependent scattering rate. This makes a comparison with the CR linewidth more difficult. For the sake of comparison we have used a scattering rate determined
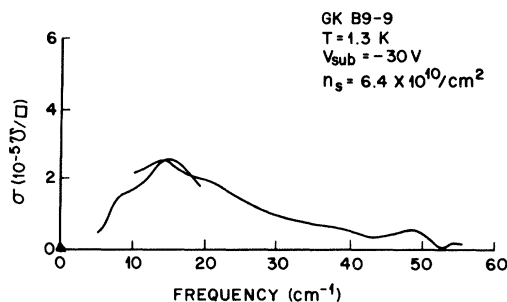
empirically by a Drude fit to the conductivity in the high-frequency region tail (the frequency region where CR is performed). As long as the scattering rate varies slowly with frequency, one would expect this method to provide a reasonable estimate of the CR linewidth in the case where the same scattering mechanisms are operative in the presence of the magnetic field.

E. Cyclotron resonance measurements

Although the main thrust of this paper is an intensive study of CR in the low n_s regime, we shall first briefly discuss our high n_s results in order to make contact with previous measurements. This is particularly important, as our experimental technique is slightly different. In contrast to other CR measurements in this system which use fixed laser frequencies and scan the magnetic field, our measurements are made with all parameters of the system held fixed. We observe the frequency response by scanning the spectrometer. This modification of the standard technique allows a direct measurement of the CR line shape at any n_s, and turns out to be crucial in developing a coherent picture of the behavior at low n_s.

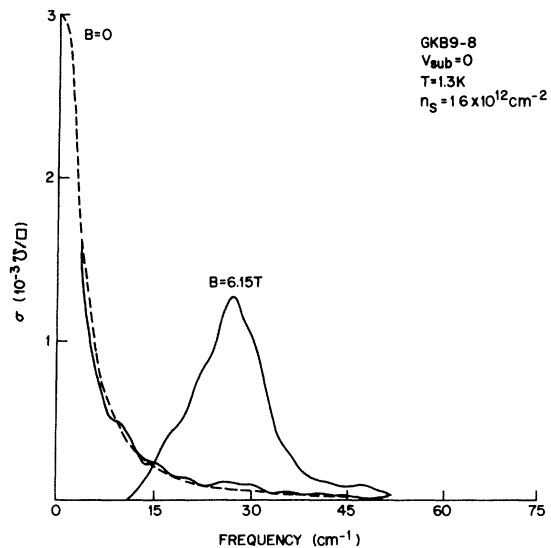A typical high-density CR line shape is shown in Fig. 5. The peak position lies below the expect-

FIG. 4. Conductivity versus frequency at n_s $= 6.4 \times 10^{10}$ cm^{-2}, $V_{sub} = -30$ V (fine structure is residual noise); $\triangle, \sigma$ (dc). The two curves represent separate spectra taken in different frequency regions with different beam splitters in the Michelson interferometer.

FIG. 5. Cyclotron resonance at $n_s = 1.6 \times 10^{12}$ cm^{-2}. $\nu = 10.7$, $B = 6.15$ T, compared to the $B = 0$ absorption at the same density. The dashed line is the theoretical Drude prediction based on the dc conductivity (fine structure is residual noise).

ed value of ω_c, giving an effective mass of
$\sim 0.2 \pm 0.01$. The line shape is asymmetric with an
absorption maximum that falls below the classical
prediction of $\frac{1}{2}$ the Drude peak by about 15%.
The integrated intensity agrees within experimental
error with the electron density calculated from the
capacitance and threshold. A positive or negative
substrate bias narrows or broadens the resonance,
respectively. A swept-field experiment at fixed
laser frequency performed on the resonance in Fig.
5 would give excess absorption on the high mag-
netic field side (corresponding to the absorption at
low frequencies here). This has been interpreted in
the past as indicative of a magnetic-field-dependent
scattering rate.[39,40] Here where the magnetic field
is fixed we can not invoke this explanation. At
present we have no explanation for the departures
from a simple classical line shape or for the dis-
placement of the peak position below the expected
cyclotron frequency.

At very low densities, however, the results are
very different. As first observed by Kennedy
et al.,[17-19] the resonance becomes extremely sharp
and is shifted in the opposite direction—to higher
frequency, lower effective mass. Figure 6 shows a
sample CR trace. At this electron density and
magnetic field, the lowest valley-spin-Landau level
is only partially filled. A comparison of the ob-
served CR with that expected for a mass $0.19m_e$
and a scattering rate determined from the Drude
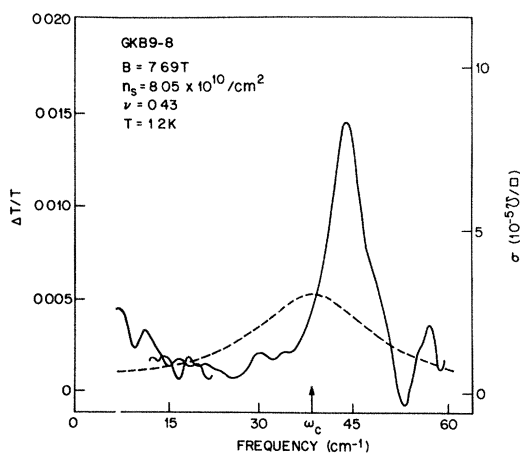line shape indicates the shift of the peak above ω_c

and the extreme narrowing of the line. The ob-
served width is ~ 5 times narrower. There is also
distinct evidence of additional absorption at low
frequency.

As the electron density is increased and the
lowest quantum state is filled, the resonance
broadens and shifts back across ω_c, as shown in
Fig. 7. This progression is apparent for a large
range of magnetic fields, but if the field is in-
creased, there is a concomitant increase in the
values of n_s over which the progression takes place.
This observation led to the crucial realization that
it is the fractional filling of the Landau quantum
states rather than the density itself which is the
critical parameter. This property proves to be fun-
damental in the analysis of possible models.

Plots of the position and width of the resonance
versus filling factor ν, then lead to universal curves
as shown in Fig. 8. Data over more than a factor
of three in magnetic fields follow this same pattern,
verifying the universal ν dependence. Data from
all of our high mobility devices could be superim-
posed on the same graph; they agree quantitatively
as well as qualitatively. This is also true of peak
position measurements published by Kennedy
et al., which are included in the figure. Lower mo-
bility samples, $\mu \sim 8000$ cm^2/V s, show a qualita-
tively similar progression occurring at the same ν
values, but the shifts are somewhat larger and the
lines broader.

We shall now discuss in more detail the pattern
that emerges as ν is increased. Below $\nu \sim 0.45$ the
behavior appears to saturate, and the resonance

FIG. 6. Cyclotron resonance $n_s = 8.0 \times 10^{10}$, $\nu = 0.43$,
$B = 7.69$ T. The solid and dash-dot curves represent
spectra taken in different frequency regions (fine struc-
ture is residual noise). Dashed line is the classical cyclo-
tron resonance derived from the scattering rate observed
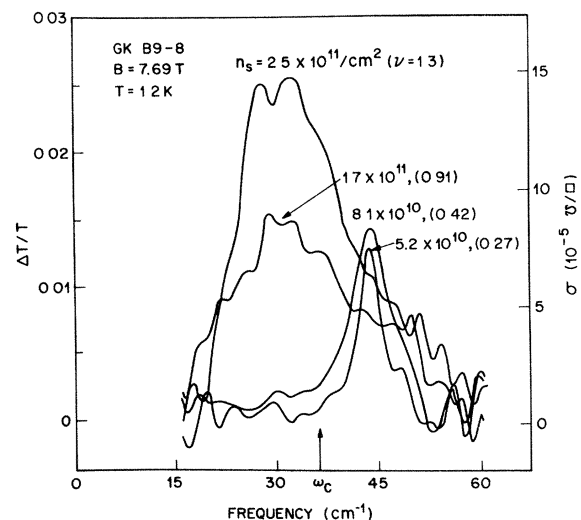in the Drude tail at $B = 0$.

FIG. 7. Evolution of CR with ν as a parameter at
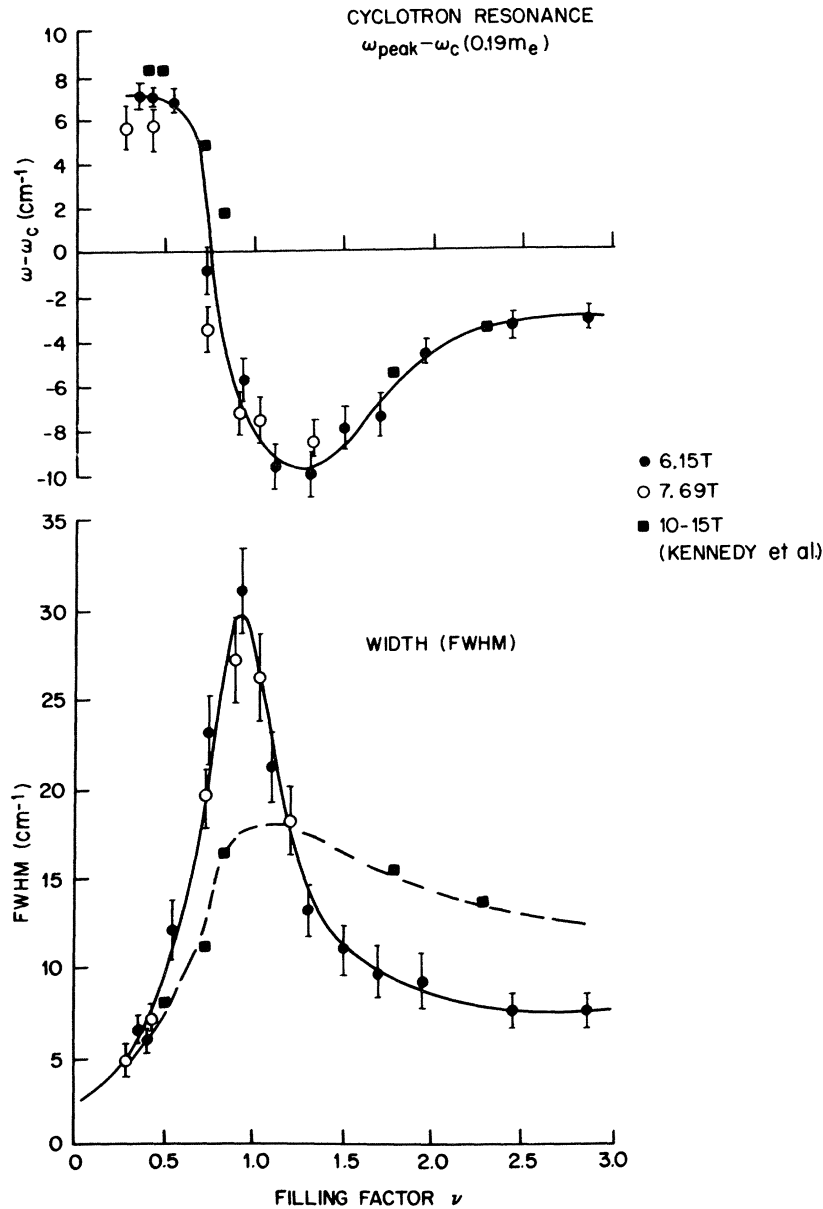$B = 7.69$ T (fine structure is residual noise).

FIG. 8. Peak position and linewidth versus ν for various magnetic fields.

takes the form shown in Fig. 6. It is extremely narrow and lies $6-8$ cm^{-1} above ω_c. There is also absorption at low frequency. We have lowered ν to less than 0.1 with no detectable change in the line shape.

As the filling factor is increased from 0.5 to 1.0 and the lowest valley is filled, the peak shifts across ω_c and the width increases by a factor of 5 or 10. In the vicinity of $\nu=1$, the resonance essentially exhibits the line shape we might have expected. The position is comparable to that observed at high electron densities and the width is approximately that predicted from the Drude tail.

Beyond $\nu=1$, the peak shifts to even lower frequency and the line shape becomes highly asymmetric. There is a sharp cutoff at low frequency and a long tail at high frequency. In this case, the full width at half maximum (FWHM) measurement is rather misleading. For $\nu \sim 1.2$, where this effect is most dramatic, the half width at half maximum (HWHM) on the low-frequency edge can be as narrow as that in the lowest ν range. Data taken at different magnetic fields indicate that, as in the case of the narrow resonance at low ν, it is the shift of the peak from ω_c that is constant, rather than the peak position itself. The effect of a re-

verse substrate bias is to broaden the low-frequency rise. The apparent shift of the peak towards ω_c is probably a result of this broadening coupled with the asymmetric line shape.

Finally, above $v \cong 1.2$ the resonance gradually approaches its high-density form, slightly below ω_c. In some samples there was a slight indication of a ripple in this monotonic approach to the high-density position in the region of $v = 2$.

F. Low-v data

Although it is clear from the foregoing discussion that interesting behavior occurs across the entire range of v, we have focused our investigation on the low-v regime, $v \leq 0.5$. As outlined in the Introduction, it is in this region that recent theoretical studies have indicated the possibility of Coulomb-induced transitions. Consequently, the remainder of the paper will focus on the behavior in this region where the resonance is anomalously narrow. We have studied the CR spectrum as a function of filling factor $(0 < v < 0.45)$, magnetic field, electric field at the interface (i.e., substrate bias effects), and temperature.

To first order, the CR line shape and position remain unchanged across the range $0.08 < v < 0.43$. Across this factor-of-five change in v, the peak position changes at most $10-20\%$. In the lowest v data, the resonance peak appears to be at a slightly lower frequency.

It is instructive to examine the position of the resonance peak as a function of magnetic field in this low-v regime. It is incorrect to ascribe the shift to higher frequency to a reduction in the effective mass m^*. On a plot of resonance position versus magnetic field, a lighter m^* corresponds to a normal linear relationship passing through the origin, but with a steeper slope. In fact, as shown in Fig. 9, although the data do appear linear in magnetic field, they do not extrapolate linearly to the origin, and the slope is actually slightly flatter, corresponding to a "mass" of $\sim 0.21 m_e$, slightly greater than m^*. It is apparently more meaningful to characterize these data as exhibiting a pinned resonance rather than a reudced effective mass. The extrapolation to zero field is added only as an aid to the eye, indicating that the shift is ~ 10 cm^{-1}, and should not be interpreted as having physical significance.

The electric field at the interface does affect the position and line shape of the resonance. By applying a substrate bias, the electric field at the in-
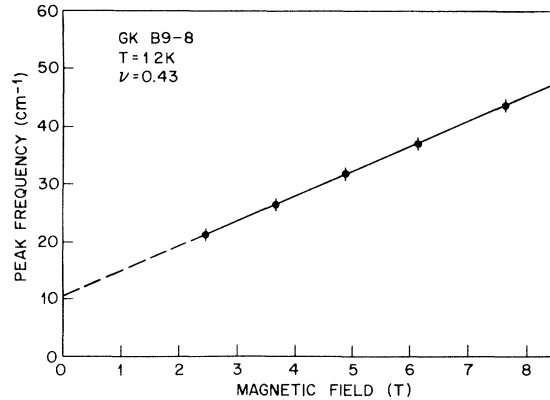

FIG. 9. Resonance position versus magnetic field at fixed v.

terface and thus the extent of the electron wave function into the substrate can be varied in a systematic way. As shown in Fig. 10, the resonance broadens and shifts to higher frequency as the electric field is increased, forcing the electrons closer to the interface. The peak height drops as the width increases so that a constant integrated area is maintained, indicating a fixed electron density. Note that the shift and width remain comparable.

This behavior may be described quantitatively by estimating the wave-function thickness for each n_s and V_{sub}, as described earlier. A plot of peak posi-
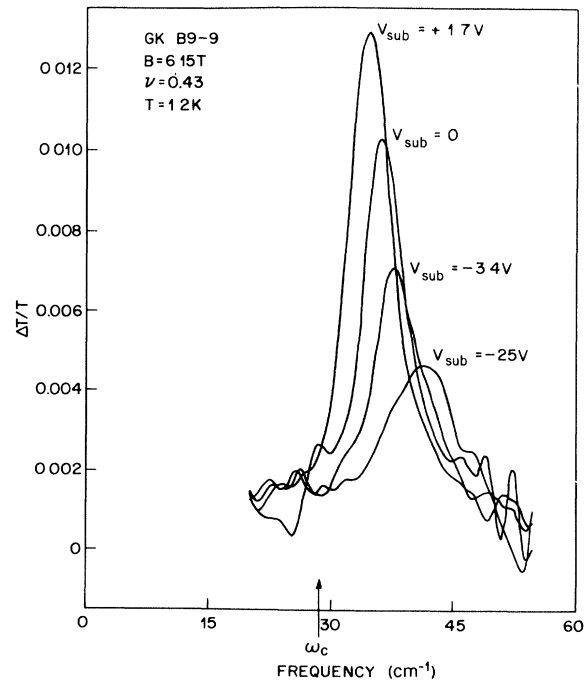

FIG. 10. Cyclotron resonance at $v = 0.43$ as a function of substrate bias (fine structure is residual noise).

tion versus inverse wave-function thickness shown in Fig. 11 exhibits an approximately linear dependence.

As the temperature is raised, the sharp resonance gradually broadens and shifts back toward ω_c. At the same time, a broad background grows, peaking approximately at ω_c. As shown in Fig. 12, this occurs gradually on a temperature scale of $5-20$ K. Unfortunately, without a specific model by which to fit the entire line shape at elevated temperatures, any empirical characterization of this process is only approximate. Within this uncertainty, we find the temperature scale insensitive to a threefold change in magnetic field or a fivefold change in n_s or v. There was an indication that increasing the electric field at the interface by a factor of 10 may have slightly increased the temperature scale, but this may merely be an effect of the electric-field-induced line shape change on the parametrization.

In summary, for $v < 0.43$ we observe a sharp resonance shifted by $6-8$ cm^{-1} to high frequency, independent of v and magnetic field. The peak position increases approximately linearly with inverse wave-function thickness, as does the width. As the filling factor is increased and the lowest valley is filled, or as the temperature is raised on the scale $5-20$ K, the sharp resonance breaks up and a broad absorption peaked at $\sim \omega_c$ appears. The temperature scale is relatively insensitive to any of the system parameters.
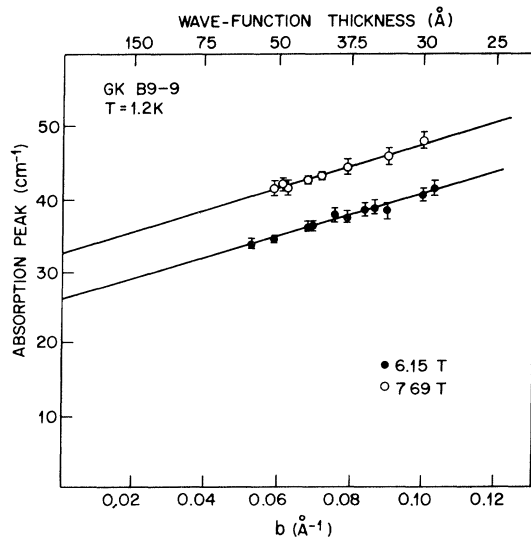
III. DISCUSSION

At present we have no single microscopic model that does a convincing job of explaining the experimental observations in a quantitative way. In its place we will discuss a number of different models, each of which is capable of describing some aspects of the observed high-frequency conductivity, but is deficient is some regard. Our attention is focused on the low filling factor $(v < 1)$ behavior. The following models will be discussed:

    A. Harmonic oscillator in a magnetic field.
    B. One-electron trapping in a random potential.
    C. Electron-phonon coupling.
    D. Pinned charge-density wave.

In the first three we ignore the interelectron Coulomb potential, working completely within a single-electron framework. Only the last model is based on collective effects due to the Coulomb interaction. Each model will be developed in turn, with the resulting predictions compared to experimental observations. Finally, in Sec. III E the implications of the observed linear dependence of the shift on the inverse wave-function thickness will be discussed.
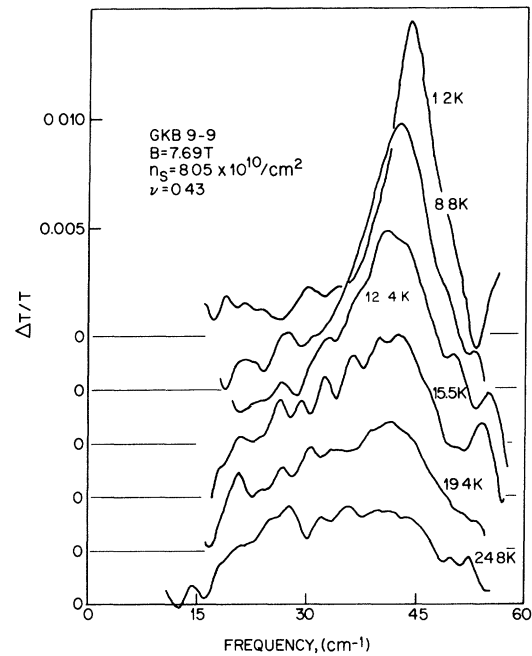

FIG. 11. Peak position versus inverse wave-function thickness normal to the interface for various magnetic fields.

FIG. 12. Evolution of CR with temperature for $v = 0.43$ (fine structure is residual noise).

A. Harmonic oscillator in a magnetic field

A classical harmonic oscillator in a magnetic field exhibits some of the features seen below $v=1$. The cyclotron resonance is shifted to higher frequency by the additional pinning potential. Further, the orbit center which could be located at will in the absence of the harmonic pinning potential now experiences a force which causes it to execute a slow anticyclonic motion about the center of the harmonic potential. This mode develops oscillator strength and increases in frequency as the pinning potential increases from zero.

We write classical equations of motion for the electron

$$m\ddot{x}+m\dot{x}/\tau+m\omega_0^2 x = e\mathscr{E}e^{i\omega t}+e\dot{y}B \ ,$$

$$m\ddot{y}+m\dot{y}/\tau+m\omega_0^2 y = -e\dot{x}B \ ,$$

(5)

where m and e are the electron mass and charge, and x and y refer to its coordinates in the plane. Motion in the z direction remains quantized in the electric subband. The electron experiences a damping rate $1/\tau$, a magnetic field B in the z direction, a harmonic pinning potential characterized by a frequency ω_0, and a linearly polarized infrared field $\mathscr{E}e^{i\omega t}$.

The resulting real conductivity $\mathrm{Re}\sigma_{xx}$ is given by

$$\mathrm{Re}\sigma_{xx}(\omega,\omega_c,\omega_0^2)=\frac{n_s e^2}{m}\frac{1}{2}\left[\frac{\omega^2/\tau}{(\omega_0^2+\omega\omega_c-\omega^2)^2+\omega^2(1/\tau)^2}+\frac{\omega^2/\tau}{(\omega_0^2-\omega\omega_c-\omega^2)^2+\omega^2(1/\tau)^2}\right] .$$

(6)

The shifted cyclotron resonance appears at

$$\omega_1\sim\omega_c/2+(\omega_c^2/4+\omega_0^2)^{1/2}$$

(7)

whereas the low-frequency anticyclotron motion of the orbit center occurs at

$$\omega_2\simeq-\omega_c/2+(\omega_c^2/4+\omega_0^2)^{1/2} \ .$$

(8)

The relative integrated strength of the two modes is given by

$$A_1/A_2=\omega_1/\omega_2 .$$

(9)

In Fig. 13 we show a typical piece of experimental data and a fit to expression (6) obtained by adjusting ω_0 and $1/\tau$ to reproduce the shifted cyclo-
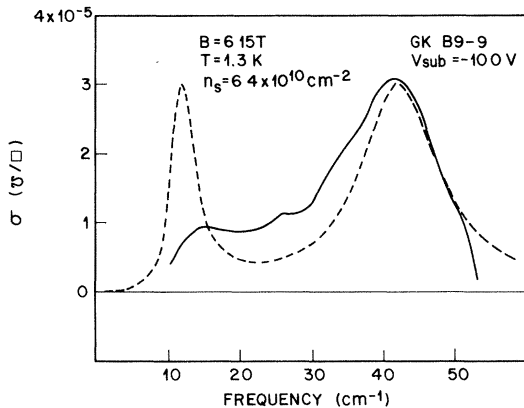
tron resonance. The sharp feature at low frequency predicted by the harmonic oscillator model is not seen in the data, although there is substantial excess low-frequency absorption.

There are other shortcomings with this model. If there were, in fact, some particular type of trap present at the interface capable of pinning inversion layer electrons as this model describes, then these effects should persist only until all the traps become filled. In this case, the critical parameter determining changes in the behavior should be the electron density itself and not the filling factor as observed. Finally, the values of ω_0 determined from the spectra reveal that the pinning potential is barely comparable to the interelectron Coulomb potential, which has been ignored in this model.

B. One-electron trapping in a random potential

The aforementioned model of identical pinning centers fails to account for the random character of the potential fluctuations at the Si-SiO$_2$ interface. As a more realistic approach, we may simulate the randomness by introducing inhomogeneous broadening to the harmonic restoring potential. Mikeska and Schmidt[41] have modeled such a pinning potential but it is clear that their model has no features that depend on v. As they point out, the critical density is fixed by the trap density and at densities above this a sharp unshifted resonance appears.

In the following we are able to go beyond the model of Mikeska and Schmidt and include the

FIG. 13. Experimental trace of CR for $v=0.43$ (fine structure is residual noise). Dashed line is the theoretical prediction of a harmonic oscillator in a magnetic field fit to the high-frequency mode.

fact that the distribution function for the restoring force experienced by a group of electrons will depend on the distribution of the electrons themselves within the inhomogeneously broadened band of states in the lowest spin-valley-Landau level. For example, the first few electrons introduced to the surface would be expected to occupy states below midband, and thus experience purely attractive potentials. The resulting CR would be shifted to higher frequency, as described earlier. In contrast, the last few electrons added to an almost filled band near $v=1$ would experience primarily repulsive potentials. Thus the introduction of inhomogeneous broadening provides a mechanism for broadening the low-frequency mode as well as explaining a filling factor rather than electron-density-dependent behavior. We develop these ideas quantitatively in the following.

We consider a random one-dimensional potential $v(x)$, which has a Gaussian distribution of amplitudes

$$D(v) = \frac{1}{(2\pi\alpha^2)^{1/2}} e^{-v^2/2\alpha^2} \tag{10}$$

where $\alpha^2 = \langle v^2 \rangle$, the mean-square deviation of the potential. We assume a Gaussian autocorrelation function for $v(r)$:

$$\langle v(r)v(r-r')\rangle = \alpha^2 e^{-r'^2/2\zeta^2}. \tag{11}$$

Then we can find the joint probability distribution for v and its second derivative $v'' = \partial^2 v/\partial x^2$

$$P(v,v'') = \frac{\zeta^2}{2^{3/2}\pi\alpha^2} e^{-v^2/2\alpha^2} e^{-(v+v''\zeta^2)^2/4\alpha^2}. \tag{12}$$

At a finite temperature T, and a fractional occupation of the first spin-valley-Landau level v, we find the Fermi level μ from the following:

$$v = \int_{-\infty}^{+\infty} dv \frac{e^{-v^2/2\alpha^2}}{(2\pi\alpha^2)^{1/2}} \frac{1}{e^{(v-\mu)/kT}+1}. \tag{13}$$

We assume that $\omega_0^2 = v''/m$. Then the inhomogeneously broadened conductivity is obtained by convolving $\mathrm{Re}\sigma_{xx}(\omega,\omega_c,\omega_0^2)$, Eq. (6), with the joint probability distribution, Eq. (12):

$$\frac{1}{v} \int_{-\infty}^{+\infty} dv \int_{-\infty}^{+\infty} dv'' \mathrm{Re}[\sigma_{xx}(\omega,\omega_c,v''/m)]$$
$$\times P(v,v'') \frac{1}{e^{(v-\mu)/kT}+1}. \tag{14}$$

We further assume there is negligible lifetime broadening $1/\tau << (\alpha/\zeta^2 m)^{1/2}$ and obtain

$$\mathrm{Re}\sigma_{xx}(\omega,\omega_c) = \frac{1}{2^{5/2}} \frac{n_0 e^2}{m} \frac{|\omega| m\zeta^2}{\alpha^2} \int_{-\infty}^{+\infty} dv\, e^{-v^2/2\alpha^2} \frac{1}{(e^{(v-\mu)kT}+1)}$$

$$\times \left[\exp\left(-\left\{\frac{v}{2\alpha} + \frac{\omega_c^2 m\zeta^2}{2\alpha}\left[\left[\frac{\omega}{\omega_c}\right]^2 - \frac{\omega}{\omega_c}\right]\right\}^2\right)\right. \tag{15}$$

$$\left. + \exp\left(-\left\{\frac{v}{2\alpha} + \frac{\omega_c^2 m\zeta^2}{2\alpha}\left[\left[\frac{\omega}{\omega_c}\right]^2 + \frac{\omega}{\omega_c}\right]\right\}^2\right)\right],$$

where n_0 is the density of electrons in the first spin-valley-Landau level and ζ is the correlation length defined in Eq. (11).

At $T=0$ the conductivity depends only on the occupancy v and the mean square of the second derivative of the potential

$$\langle v''v'' \rangle = \frac{3\alpha^2}{\zeta^4}. \tag{16}$$

We use a frequency parameter $\beta = (\alpha/m\zeta^2)^{1/2}$ to describe the resonance at $T=0$. This is the only parameter at our disposal at $T=0$ K.

In Fig. 14 we show a typical data for $v=0.43$, $H=61.5$ kG, and $T=1.3$ K with a substrate bias of -10 V. Overlaid on the experimental data is expression (15) with $\beta=20$, 15, and 10 cm^{-1}. Quantitative agreement is lacking but the essential features are there—a shifted cyclotron resonance and a low-frequency mode substantially broader than obtained with the classical, lifetime-broadened harmonic oscillator.
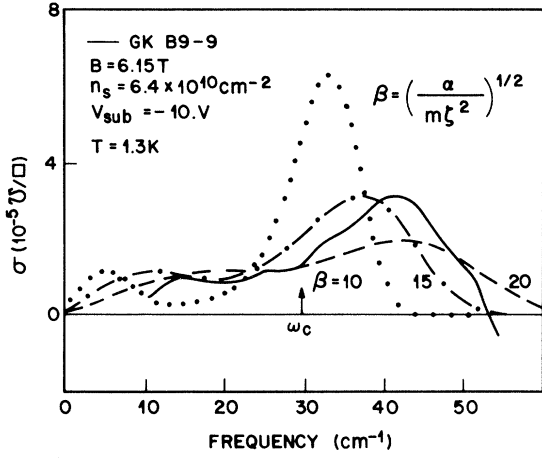
It is interesting to explore the v and temperature

FIG. 14. Theoretical CR line shape with β $=(\alpha/m\zeta^2)^{1/2}$ as a parameter based on an inhomogeneously broadened ground-state spin-valley-Landau level. Solid line is a typical expt. trace (fine structure is residual noise).

FIG. 16. Evolution of the Cr line shape with T derived from a model of an inhomogeneously broadened ground-state spin-valley-Landau level.

dependence of this line shape (Figs. 15 and 16). In both cases the spectrum moves to lower frequencies and broadens, but the behavior predicted by the model is far less dramatic than that seen experimentally. Both at high temperatures and near $\nu=1$ the model still allows a substantial fraction of electrons to be trapped in the lower part of the band, retaining the low-frequency pinned mode. The experimental data is quite the opposite. The low-frequency mode disappears at elevated temperature and above $\nu=0.5$. There is no evidence of
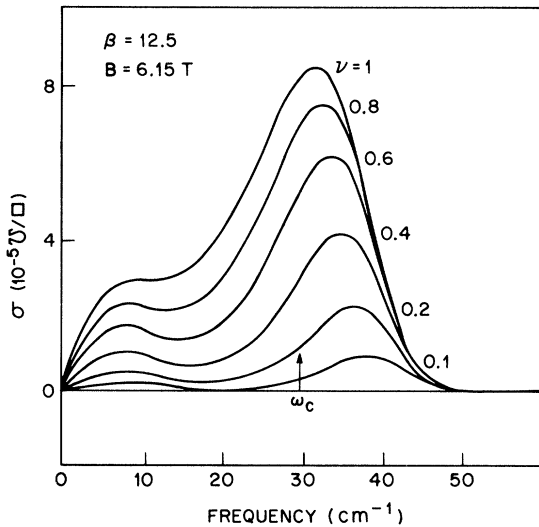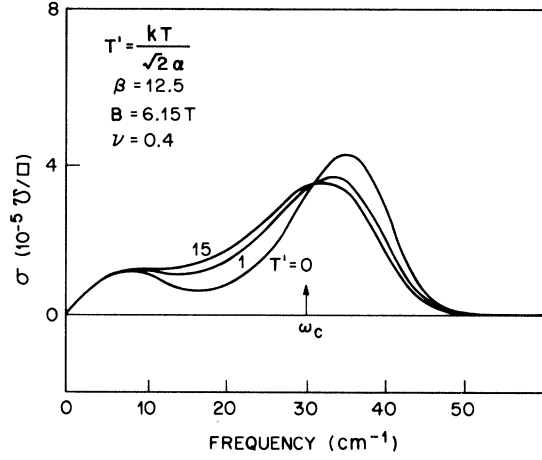
pinning or trapping of electrons at $\nu=1$ or at elevated temperatures in the experimental data.

C. Electron-phonon coupling

For fractional occupation of the lowest level less than $\frac{1}{2}$ one can constract a ground state in which the electrons do not substantially overlap. Under these conditions the electron may conceivably form its own potential well by driving a local lattice distortion. For high-frequency oscillations of the electron, the relaxation time of the local deformation is too slow, and the electron will appear to be bound, resulting in a pinned CR. Further, as the level is completely filled the wave functions will begin to overlap and the spatial variation of the local deformation will be washed out. Thus both the shifted CR and the ν dependence develop in a natural way within this model. To explore this point of view quantitatively, consider the deformation-potential energy

$$U=\tfrac{1}{2}(Eu^2)+\Xi\rho u$$

where E is the elastic constant for Si $\sim 10^{11}$ J/m^3, Ξ is the deformation potential ~ 9 eV, ρ is the quantum-mechanical electron density $\sim |\psi|^2$ in the region of the deformation, and u is the strain. This is clearly a gross simplication of the electron lattice coupling, but the essential features will emerge.

The substrate will produce a local strain u that will minimize the energy U and result in a net gain in energy

FIG. 15. Evolution of the CR line shape with ν derived from a model of an inhomogeneously broadened ground-state spin-valley-Landau level.

$$\Delta U \sim \frac{\Xi^2 \rho^2}{E} . \tag{17}$$

Now ρ may be estimated to be

$$\rho \sim \frac{1}{\langle z \rangle} \frac{1}{\pi l^2} , \tag{18}$$

where $\langle z \rangle$ is the average wave-function thickness normal to the interface and l is the cyclotron radius.

We assume this deformation cannot follow high-frequency oscillations of the electrons, and to first order exerts a harmonic binding potential

$$\Delta U \sim \frac{1}{2} \frac{\Xi^2}{\pi E \langle z \rangle} \frac{r^2}{l^4} , \tag{19}$$

where r represents the distance from the center of the deformation. This results in a harmonic pinning frequency

$$\omega_0 = \left[\frac{\Xi^2}{\pi E \langle z \rangle} \left[\frac{1}{l^4 m^*} \right] \right]^{1/2} \tag{20}$$

For $\langle z \rangle \sim 50$ Å and $l \sim 81$ Å $(B = 10$ T) we calculate $\omega_0 \sim 7$ cm^{-1}. To bring ω_0 into the range of experiment requires a deformation-potential coupling at the surface more than 3 times larger than that found in the bulk. There is an even more serious defect to this particular model. Solving for the high-frequency mode

$$\omega = \frac{\omega_c}{2} \left[1 + \left[1 + \frac{4 \Xi^2 m}{\pi \langle z \rangle E \hbar^2} \right]^{1/2} \right] , \tag{21}$$

we see that it varies with magnetic field in such a way that the resonance extrapolates to zero at zero magnetic field. In other words, the behavior appears as a mass shift rather than a pinned resonance, as observed.

We further note that low-mobility samples give larger pinning parameters. If the deformation potential were responsible, we would be forced to admit not only unreasonably large values for Ξ but a dependence of the deformation potential on the sample that is not found in the literature.

D. Pinned charge-density wave

It seems likely that electron correlations are playing an interesting role in determining the ground state of this system in the extreme quantum limit. At densities $\sim 5 \times 10^{10}$/cm^2 the Coulomb energy is approximately $E_c = (e^2/4\pi\bar{\epsilon})$ $\times \sqrt{n_s} \sim 45$ K, and one of the most important energies in the problem. Here $\bar{\epsilon}$ is the average dielectric permittivity of Si and the oxide. In the following we explore the possibility that in the extreme quantum limit at low temperatures, the electrons execute zero-point motion about their orbit centers, which are in turn arranged to minimize the Coulomb interaction energy. It is widely appreciated that in arbitrarily large magnetic fields the only remaining degree of freedom is the motion of the orbit centers, and that these behave as a collection of classical particles. It has been shown experimentally[2] and theoretically[20-25] that at sufficiently low temperatures such classical particles interacting via their mutually repulsive Coulomb interaction will crystallize into a Wigner solid. In this instance, however, the ordering temperature is expected to be less than 1 K, well below the temperatures covered in these experiments. If one insists that some sort of correlated behavior is being seen, then we can ask for no more than short-range order.[12]

We assume then that at low temperatures and at $\nu < 0.5$ the electrons arrange themselves in such a way as to avoid each other. Since the fractional occupancy is less than 0.5, there can be deep minima in the charge density[9] between the orbit centers, and the electron density will be modulated with a period of the electron spacing—an incipient Wigner condensate if you will. In this sense we will refer to the ground state as a charge-density-wave state and explore the consequences of such a starting hypothesis.

Fukuyama and Lee[42] have developed a model for a pinned 2D charge-density wave in a magnetic field that can be used with some success. They assume a 2D charge-density wave given by

$$\rho(r) = n_s + \rho_0 \{ \cos[Qx + \phi_x(\vec{r})]$$
$$+ \cos[Qy + \phi_x(\vec{r})] \} , \tag{22}$$

where n_s is the average density and ρ_0 the amplitude of the modulation. We take Q, the wave vector for the square array, to be $2\pi\sqrt{n_s}$. The excitations of this system are described by the spatial variations of the phase, $\phi_x(r)$, $\phi_y(r)$.

The charge-density wave, CDW, is assumed pinned by random delta-function potentials $v_0 \delta(\vec{r} - \vec{r}_i)$ and the net interaction potential experienced by the CDW is written as

$$v = e V_0 \rho_0 \sum_i \{ \cos[Qx_i + \phi(\vec{r}_i)]$$
$$+ \cos[Qy_i + \phi(r_i)] \} . \tag{23}$$

Another ingredient is a phenomenological elastic

constant C_0 such that the elastic energy of these phase variations can be written

$$U = \tfrac{1}{2}C_0 \sum_{\alpha,\beta} \int d^2 r \left[\frac{d\phi_\beta}{d\chi_\alpha} \right]^2 . \tag{24}$$

The correlation length L_0 for short-range order is related to the pinning potential and the elastic energy for shear distortions by

$$L_0 \approx \frac{4C_0}{eV_0\rho_0\sqrt{n_i}} . \tag{25}$$

[In using (25) we depart from the development outlined by Fukuyama and Lee with special dispensation from the authors. The original expression (3.12) in Ref. 42 required the lattice to gain pinning energy at the expense of both shear and compressional distortions. The latter involve the long-range Coulomb interaction and are relatively stiff. By allowing the system to minimize its total energy at the expense of shear distortions only, expression (25) is obtained and we use it in the following. See also Ref. 43.]

The current-carrying excitations of the system are pinned with a complex pinning parameter $\gamma^2(1 + ia)$ where a is of the order of unity and γ is given by

$$\gamma = [(eV_0\rho_0\sqrt{n_i}/L_0)(Q^2/n_s m^*)]^{1/2} . \tag{26}$$

The frequency-dependent conductivity may be derived

$$\sigma_{xx}(\omega) = \frac{i\omega[\omega^2 - \gamma^2(1+ia)]n_s e^2/m^*}{[\omega^2 - \gamma^2(1+ia)]^2 - \omega_c^2\omega^2} . \tag{27}$$

The qualitative features of (27) are essentially the same as the harmonic oscillator, a shifted cyclotron resonance and low-frequency oscillation of the orbit centers about the pinning potentials. The damping, however, which is determined by the imaginary part of $\gamma^2(1 + ia)$ leads to much broader low-frequency modes and remarkably good fits to the observed data. Figures 17(a) and 17(b) show two sample least-squares fits to the data taken on high-mobility samples. We emphasize that the only adjustable parameters that we have at our disposal are γ and a. The vertical scale has not been adjusted. The broader, more shifted resonances observed in our lower mobility samples, $\mu \sim 8000$ cm^2/V s, yield correspondingly larger values of γ, but the fits are noticeably less satisfactory.

In Fig. 18 we plot values obtained for γ from two different high-mobility samples as a function
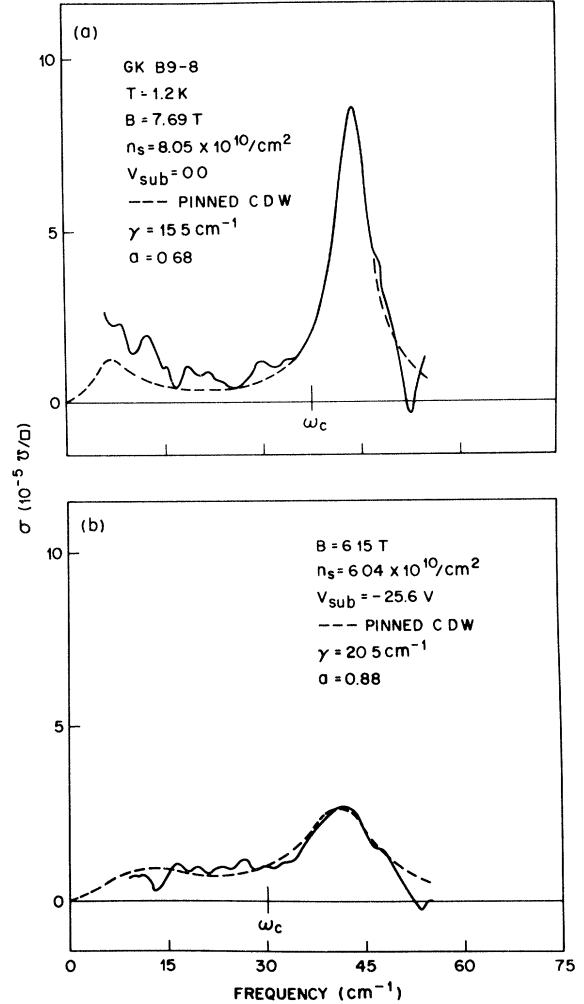

FIG. 17. Least-squares fit of the CR line shape to pinned CDW model of Fukuyama and Lee (Ref. 42): (a) $V_{sub}=0.0$ V; (b) $V_{sub}=-25.6$ V (fine structure is residual noise).

of the inverse wave-function thickness normal to the interface. A straight line passing through the origin can easily be drawn through the data, implying that the pinning is related to random interface potentials. It is apparent that this phenomenology based on random pinning of a 2D charge-density wave in a magnetic field can easily explain the observed resonance features for $v<0.5$ and enables us to extract an interface pinning parameter γ. Although the phenomenology of Fukuyama and Lee makes no statement on how the pinned resonance will depend on v, there is ample theoretical justification for the notion that the CDW may vanish at $v=1$.[11] If $\rho_0=0$ in Eq. (26), γ will also vanish and we would expect to recover an unshifted resonance
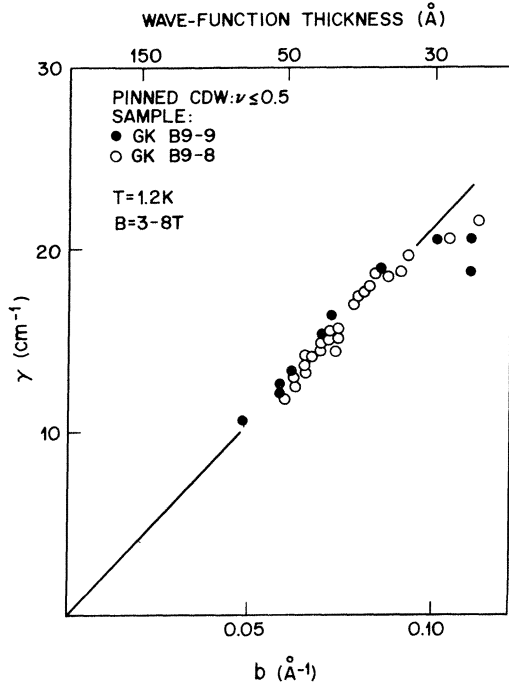
WAVE-FUNCTION THICKNESS (Å)

FIG. 18. γ versus inverse wave-function thickness normal to the interface.

at $\nu=1$. The theory offers no predictions for the behavior for $\nu>1$.

There are some serious weaknesses in the model. First, the shift and linewidth do not change appreciably as $\nu\rightarrow0$. Further, one might also expect the temperature at which the shifted resonance is lost to depend on filling factor and possibly on the Coulomb interaction through n_s and/or the pinning strength through the electric field at the interface. Our data, although difficult to parametrize accurately without a specific model, show a disturbing lack of significant dependence on any of these parameters. One possible explanation of this discrepancy is that thermal excitation to a higher-lying state (the other valley for example) of fixed energy is responsible for the breakup of the CDW. It is also possible that the competing influences of parameters predicted by the theory lead to a rough cancellation.

To more critically test the relevance of this model we can extract estimates of the modulation depth ρ_0/n_s and the correlation lenght L_0. By eliminating $eV_0\sqrt{n_i}$ from Eqs. (25) and (26) we can find an expression relating L_0 to the pinning frequency γ:

$$L_0=(4\pi/\gamma)(C_0/m^*)^{1/2}. \tag{28}$$

For an approximation of the elastic constant C_0, we use the value appropriate for a true Wigner solid. This we obtain by a comparison of the transverse-mode dispersion relations

$$\omega_t^2=(C_0Q^2/n_sm^*)q^2\text{—pinned CDW, Ref. 41} \tag{29}$$

$$\omega_t^2=\left[\frac{e^2}{8\pi^5\epsilon d}\frac{Q^2}{n_sm^*}\right]q^2\text{—Wigner solid}$$

where d is the interelectron spacing. By inspection,

$$C_0=\frac{e^2}{8\pi^5\epsilon d}. \tag{30}$$

At an electron density of 8×10^{10} cm^2 we obtain correlation lengths for short-range order that vary from $326-160$ Å as the pinning frequency varies from 10 to 20 cm^{-1}. The charge-density wave is highly disordered. In fact, the correlation length is so short that it raises serious doubts as to the quantitative validity of the model which assumes $L_0>>d$.

From γ we can determine the product of the scattering potential $eV_0\sqrt{n_i}$ and the charge-density amplitude ρ_0:

$$\rho_0(eV_0\sqrt{n_i})=\frac{\gamma}{\pi}(m^*C_0)^{1/2}. \tag{31}$$

By estimating the scattering potential $eV_0\sqrt{n_i}$ from the momentum scattering in the Drude tail we can determine the modulation depth ρ_0/n_s. We assume that the high-frequency $(30-50$ cm$^{-1})$ Drude is given by $\sim(n_se^2/m)[1/1+(\omega\tau_p)^2]$. Then in zero magnetic field at 8×10^{10} the momentum scattering rate is $(2\pi c\tau_p)^{-1}\sim20$ cm^{-1}. With $n_iV_0^2e^2=\hbar^3/m^*$ $1/\tau_p$ we estimate

$$\rho_0/n_s\sim0.25. \tag{32}$$

The interesting point here is not the exact value but that the model does require physically reasonable values, i.e., $\rho_0/n_s\leq1$. If L_0 casts doubt on the model's applicability, the reasonable value of ρ_0/n_s lends credibility.

It is perhaps worth remarking here that the linewidth for the pinned CDW should be understood in terms quite different from the transport scattering rate $1/\tau_p$. An entity with dimensions of the order of the correlation length moves in phase and effectively experiences an average pinning potential. From Eq. (26) we see that because of this

averaging in the case of $L_0 \to \infty$ the pinning parameter goes to zero whatever the strength of the scattering centers. In this sense the cyclotron resonance may be viewed as being "exchange narrowed" by the strong Coulomb interaction between electrons.

The picture that emerges from fitting this model to the experiment is one of a highly disordered modulation of the charge density. The correlation length for short-range order is of the same order as the electron spacing, which implies that the disordering potential is as important as the electron-electron interaction. Indeed, if we estimate the relative strengths of the two terms by comparing the 2D plasmon frequency ω_p at a wavelength comparable to the interparticle spacing, to the pinning frequency γ, we find them comparable:

$$\omega_p \sim 64 \text{ cm}^{-1}, \quad \gamma \sim 20 \text{ cm}^{-1} .$$

Alternately we may use the parameter used by Aoki[10] which is the ratio of the Coulomb energy to the bandwidth. The Coulomb energy at $8 \times 10^{10}/\text{cm}^2$ is about 4 meV. The bandwidth is $\Gamma = 4(eV_0\sqrt{n_i})\sqrt{n_0}$, where n_0 is the degeneracy of the first spin-valley-Landau level. Assuming a momentum scattering of 20 cm^{-1} we obtain $\Gamma \sim 4$ meV and a ratio of $E_C/\Gamma \sim 1$ [see Ref. 10, Figs. 1(b) and 1(c)]. The fact that the correlation length is extremely short is consistent with the above estimates of the relative strengths of the disordering potential and Coulomb interaction.

E. Pinning by random strain

Irrespective of the choice of model, the experimental data requires an essentially linear dependence of the pinning frequency on the inverse wave-function thickness. The dependence shows the least scatter for values of γ obtained from fits to the pinned CDW model, which is not surprising as this model also reproduces the line shapes most accurately. This linear dependence would appear to provide a clue as to the source of the pinning potential. If the potential $v(r,z)$ is short ranged in r with a strength $V_0 = \int d^2r \, v(r,z)$, that falls off like $1/z$ as we leave the interface, then we would quite simply recover a linear dependence on b or $1/\langle z \rangle$ which would dominate the behavior of γ.

To see this, we substitute L_0 from (25) into (26) and obtain for γ

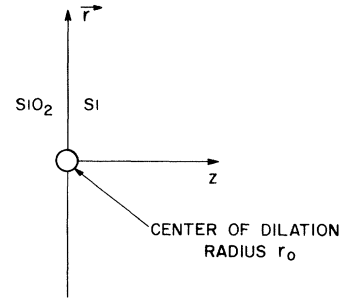$$\gamma = eV_0\rho_0\sqrt{n_i} \frac{\pi}{(m^*C_0)^{1/2}} . \tag{33}$$

FIG. 19. Geometrical factors relating to the scattering by a point lattice deformation at the interface.

If $v(r,z) \propto \delta(r)1/z$ then

$$V(r) \propto \delta(r) \int_0^\infty \psi(z)^2 \frac{1}{z} dz \tag{34}$$

and

$$V_0 \propto 1/\langle z \rangle . \tag{35}$$

(To obtain a linear relation we must also assume that neither ρ_0 or C_0 is a strong function of $\langle z \rangle$.)

Scattering by random strains leads to a scattering potential of the form (35). Consider a small center of dilation at the interface. We characterize the dilation by a void of radius r_0 which pushes the lattice away from a particular point (see Fig. 19). The exact form of the local perturbation is not crucial, but for the sake of simplicity we assume a spherical void. If we further ignore the difference in elastic properties of the Si and SiO_2, we can write down the potential seen by an elec-
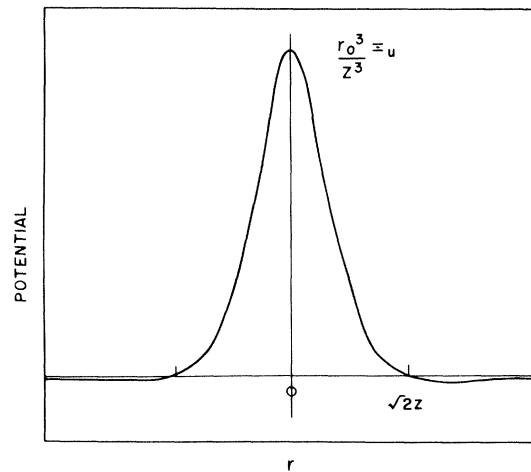

FIG. 20. Pinning potential near a point dilation at the interface as a function of r in a plane located z from the interface.

tron in the vicinity of this perturbation[44]:

$$v(r,z) = \frac{1}{2}\frac{r_0^3}{z^3}\Xi_u \left[\frac{3}{[(r/z)^2+1]^{5/2}} - \frac{1}{[(r/z)^2+1]^{3/2}} \right], \quad (36)$$

where Ξ_u is the deformation potential for silicon (~ 9 eV).

The amplitude of the potential varies like $1/z^3$ and has a length scale in the plane parallel to the interface which varies with z (see Fig. 20). Although the total integrated strength of the potential is zero, the strength of the central peak is

$$\int_0^{r=z} v(r,z)2\pi r \, dr = \frac{8\pi}{3^{1/2}}\frac{r_0^3}{z}\Xi_u \quad (37)$$

and we approximate $v(r,z)$ by

$$\frac{8\pi}{3^{1/2}}\frac{r_0^3}{z}\Xi_u \delta(r) \quad (38)$$

Carrying out the z average

$$v(r) = \int_0^\infty dz \, \frac{b^3}{2}z^2 e^{-bz} v(r,z), \quad (39)$$

we obtain

$$v(r) = \frac{4\pi}{3^{1/2}}r_0^3 b\,\Xi_u \delta(r). \quad (40)$$

Substituting into (33) and assuming $\rho_0 = (0.25)n_s$ we obtain

$$\gamma = \frac{\pi^2}{3^{1/2}}(r_0^2\sqrt{n_i})n_s\frac{\Xi_u}{(mC_0)^{1/2}}b. \quad (41)$$

The solid line in Fig. 18 is obtained for $r_0^3\sqrt{n_i} = 4.9\times10^{-22}$ m^2. For an effective void radius of 2 Å we require a density of point defects on the surface equal to $n_i = 3.8\times10^{11}$/cm^2, which is not unreasonable. Inhomogeneous strains are thought to be a source of interface state density in the Si band gap and inversion layer band tailing.[45] While the above exercise is not unambiguous, it does indicate that such perturbations at the interface could give rise to the pinning that we see in these samples.

At this stage we return to a point that we made earlier. Samples with lower peak mobilities at 4.2 K exhibit much larger shifts and pinning parameters. It may be unrealistic to assume that the same scattering mechanism that depresses the peak mobility at electron densities of the order of 10^{12}/cm^2 is responsible for the low-density pinning, but our limited sample experience would appear to indicate

a correlation. The accepted scattering mechanism for $n_s \lesssim 10^{12}$/cm^2, the one thought to depress the peak mobility, is charged impurity scattering. It is clear that the effects we describe here, however, cannot be modeled by such a strong binding potential. Coulomb centers at the interface are thought to have binding energies of the order of 20 meV as compared to the pinning energies of $1-2$ meV we require.

IV. CONCLUSIONS

From the discussion of models in the previous section it is clear that at the present time no single model can adequately describe all of the observed features. With interelectron Coulomb interactions comparable to or greater than other relevant forces, it would seem unlikely that a satisfactory model could be constructed without including collective effects. Consequently, it is not surprising that the first three models described, which are based solely on single-electron pictures, should all suffer major shortcomings.

Trapping of electrons at individual pinning centers is capable of generating sharp, shifted CR line shapes and additional low-frequency absorption, as demonstrated in the harmonic approximation. Nevertheless, any model based on specific electron trap sites cannot reproduce the critical dependence on ν, a basic requirement for the credibility of any model. The introduction of random potentials at the interface allows the ν dependence to enter naturally and also adds inhomogeneous broadening to the low-frequency mode. Random potentials cannot, however, explain the observed evolution of the line shape with ν, since even at $\nu=1$, half of the electrons should continue to experience positive restoring forces and exhibit a pinned cyclotron resonance. Electron-phonon coupling leading to polaron self-trapping was also shown to generate a shifted CR and a ν dependence related to wave-function overlap. The predicted shift of the resonance should be proportional to B, however, and should appear as a mass shift contrary to experiment. Furthermore, the data would require a sample-dependent electron-phonon coupling some 3 times larger than in the bulk.

White and Ngai[46] have proposed a trapping model that requires electron-electron interactions via a negative-U center. However, this seems inappropriate here since the strong magnetic field has lifted the spin degeneracy and the exclusion princi-

ple then forbids the double occupancy needed to bind two electrons at a locally distorted site. Further, the trapping density would still depend on the density of such sites and not on the degeneracy of the first spin-valley-Landau level.

All single-electron models ignore the fact that the pinning energies determined from fits to the data are in all cases smaller than the relevant Coulomb interaction energy. The fourth and final model, that of a pinned CDW, deals directly with the large Coulomb interactions. This model based on collective effects was found to provide remarkably good fits to all the CR line shapes as well as reasonable values of the pinning frequency and damping and the CDW amplitude. The coherence length determined within this model is only on the order of the interelectron spacing, too short to be consistent with approximations made within the theory. It is not valid to characterize the system as a CDW with correlation extending over many interelectron spacings and over many pinning centers. It appears, instead, that the pinning centers distort the Coulomb-induced ordering to such an extent that only very short-range order persists.

The picture of the 2D electron gas in the extreme quantum limit that emerges from these experiments and this theoretical modeling might be described as that of a highly disordered Wigner glass.[10] The Coulomb interactions appear strong enough to produce substantial ordering of the electrons, but interactions with the interface distort the array, leaving only short correlation lengths on the order of the interelectron spacing. The Wigner glass manifests itself by a narrowed CR resonance line shape. Interactions of this amorphous system with the interface then shift the resonance to higher frequency and introduce additional low-frequency absorption associated with local collective modes. Since the cyclotron energy, Coulomb energy, and pinning energy are all roughly comparable, we can not extract reliable quantitative parameters describing the electron gas, or conversely, make truly rigorous tests of the CDW model. To gain the latter two goals we must wait upon either substantially higher mobility devices in larger magnetic fields or more sophisticated theory that is able to more realistically treat the current experimental situation.

[1]E. P. Wigner, Phys. Rev. 46, 1002 (1934).
[2]C. C. Grimes and G. Adams, Phys. Rev. Lett. 42, 795 (1979).
[3]In three dimensions, see W. G. Kleppmann and R. J. Elliot, J. Phys. C 8, 2729 (1975).
[4]Y. E. Lozovik and V. I. Yudson, Zh. Teor. Fiz. Pis'ma Red. 22, 26 (1975) [Sov. Phys.—JETP Lett. 22, 11 (1975)].
[5]H. Fukuyama, Solid State Commun. 19, 551 (1976); 17, 1323 (1975).
[6]M. Tsukada, J. Phys. Soc. Jpn. 42, 391 (1977).
[7]M. Tsukada, J. Phys. Soc. Jpn. Lett. 40, 1515 (1976).
[8]Y. Kuramoto, J. Phys. Soc. Jpn. Lett. 44, 1035 (1978).
[9]Y. Kuramoto, J. Phys. Soc. Jpn. 45, 390 (1978).
[10]H. Aoki, J. Phys. C 21, 633 (1979).
[11]D. Yoshioka and H. Fukuyama, J. Phys. Soc. Jpn. 47, 394 (1979).
[12]H. Fukuyama, P. M. Platzman, and P. W. Anderson, Surf. Sci. 73, 374 (1978); Phys. Rev. B 19, 5211 (1979).
[13]H. Fukuyama, Technical Report of ISSP Series A No.

993 (1979).
[14]S. Kawaji and J. Wakabayashi, Solid State Commun. 22, 87 (1977).
[15]S. Kawaji and J. Wakabayashi, Surf. Sci. 58, 238 (1976).
[16]D. C. Tsui, Solid State Commun. 21, 675 (1977).
[17]T. A. Kennedy, R. J. Wagner, B. D. McCombe, and D. C. Tsui, Solid State Commun. 22, 459 (1977).
[18]R. J. Wagner, T. A. Kennedy, B. D. McCombe, and D. C. Tsui, Phys. Rev. B 22, 945 (1980).
[19]R. J. Wagner and D. C. Tsui, J. Magn. and Magn. Mater. 11, 26 (1979).
[20]J. M. Kosterlitz and D. J. Thouless, J. Phys. C 6, 1181 (1973).
[21]D. J. Thouless, J. Phys. C 11, L189 (1978).
[22]B. I. Halperin and D. R. Nelson, Phys. Rev. Lett. 41, 121 (1978); 41, 519(E) (1978).
[23]D. R. Nelson and B. I. Halperin, Phys. Rev. B 19, 2457 (1979).
[24]A. P. Young, Phys. Rev. B 19, 1855 (1979).
[25]R. H. Morf, Phys. Rev. Lett. 43, 931 (1979).

[26]G. Abstreiter, P. Kneschaurek, J. P. Kotthaus, and J. F. Koch, Phys. Rev. Lett. 32, 104 (1974).

[27]S. J. Allen, Jr., D. C. Tsui, and J. V. Dalton, Phys. Rev. Lett. 32, 107 (1974).

[28]J. P. Kotthaus, Surf. Sci. 73, 472 (1978).

[29]J. P. Kotthaus, G. Abstreiter, J. F. Koch, and R. Rauvaud, Phys. Rev. Lett. 34, 151 (1975).

[30]G. Abstreiter, J. P. Kotthaus, J. F. Koch, and G. Dorda, Phys. Rev. B 14, 2480 (1976).

[31]T. A. Kennedy, R. J. Wagner, B. D. McCombe, and D. C. Tsui, Phys. Rev. Lett. 35, 1031 (1975).

[32]G. Abstreiter, J. F. Koch, P. Goy, and Y. Couder, Phys. Rev. B 14, 2494 (1976).

[33]H. Kühlbeck and J. P. Kotthaus, Phys. Rev. Lett. 35, 1019 (1975).

[34]P. Stallhofer, J. P. Kotthaus, and J. F. Koch, Solid State Commun. 20, 519 (1976).

[35]B. A. Wilson, S. J. Allen, Jr., and D. C. Tsui, Surf. Sci. 98, 262 (1980).

[36]B. A. Wilson, S. J. Allen, Jr., and D. C. Tsui, Phys.

[37]D. C. Tsui, S. J. Allen, Jr., R. A. Logan, A. Kamgar, and S. N. Coppersmith, Surf. Sci. 73, 419 (1978).

[38]F. Stern and W. F. Howard, Phys. Rev. 163, 816 (1967).

[39]G. Abstreiter, J. P. Kotthaus, J. F. Koch, and G. Dorda, Phys. Rev. B 14, 2480 (1976).

[40]T. Ando, J. Phys. Soc. Jpn. 38, 989 (1975).

[41]H-J. Mikeska and H. Schmidt, Z. Phys. B 20, 43 (1975).

[42]H. Fukuyama and P. A. Lee, Phys. Rev. B 18, 6245 (1978).

[43]D. J. Bergman, T. M. Rice, and P. A. Lee, Phys. Rev. B 15, 1706 (1977).

[44]A. E. H. Love, A Treatist on the Mathematical Theory of Elasticity (Cambridge University Press, Cambridge, 1892), p. 183 ff.

[45]R. B. Laughlin, J. D. Joannopoulos, and D. J. Chadi, Phys. Rev. B 21, 5733 (1980).

[46]C. T. White and K. L. Ngai, Surf. Sci. 98, 227 (1980).

Rev. Lett. 44, 479 (1980).